





Cite this: *RSC Adv.*, 2019, 9, 11996

Interfacial electronic structure between a W-doped In_2O_3 transparent electrode and a V_2O_5 hole injection layer for inorganic quantum-dot light-emitting diodes

Su Been Heo,^a Jong Hun Yu,^a Minju Kim,^b Yeonjin Yi,^b Ji-Eun Lee,^c Han-Ki Kim ^c and Seong Jun Kang ^{*a}

The interfacial electronic structure between a W-doped In_2O_3 (IWO) transparent electrode and a V_2O_5 hole injection layer (HIL) has been investigated using ultraviolet photoelectron spectroscopy for high-performance and inorganic quantum-dot light-emitting diodes (QLEDs). Based on the interfacial electronic structure measurements, we found gap states in a V_2O_5 HIL at 1.0 eV below the Fermi level. Holes can be efficiently injected from the IWO electrode into poly[(9,9-dioctylfluorenyl-(2,7-diy))]-co-(4,4'-(4-sec-butylphenyl)diphenylamine) (TFB) through the gap states of V_2O_5 , which was confirmed by the hole injection characteristics of a hole-only device. Therefore, conventional normal-structured QLEDs were fabricated on a glass substrate with the IWO transparent electrode and V_2O_5 HIL. The maximum luminance of the device was measured as 9443.5 cd m^{-2} . Our result suggests that the IWO electrode and V_2O_5 HIL are a good combination for developing high-performance and inorganic QLEDs.

Received 28th February 2019

Accepted 11th April 2019

DOI: 10.1039/c9ra01520e

rsc.li/rsc-advances

Introduction

Light-emitting diodes based on electroluminescence from quantum-dots are one of the most promising devices as next-generation displays due to the narrow emission spectrum characteristics and the high luminous efficiency.^{1–3} Quantum-dot light-emitting diodes (QLEDs) can be fabricated using a low-cost solution process that enables a large-scale flexible display.⁴ Moreover, the band gap of quantum-dots (QDs) is controllable by changing the dimensions of QDs due to the quantum confinement effect.⁵ Therefore, full-color QLEDs and white QLEDs have been successfully demonstrated.^{6–8}

Conventional indium-tin-oxide (ITO) film is the most commonly used transparent electrode for light-emitting diodes and photovoltaics.^{9,10} Sputtered ITO films have a low sheet resistance and high carrier mobility with a high carrier concentration.¹¹ Although a high process temperature (300 °C) is required to form an ITO film with a high conductivity, ITO is a typical transparent electrode to fabricate QLEDs.¹² Generally, ITO is used as a transparent electrode and poly(3,4-ethylenedioxythiophene):poly(styrenesulfonate) (PEDOT:PSS) is

used as a hole injection layer (HIL) for the QLEDs.¹³ However, the hygroscopic and acidic nature of PEDOT:PSS can damage the surface of the ITO, and degrade device performance parameters such as the electroluminescence (EL) and life-time of the device.¹⁴ Therefore, ITO and PEDOT:PSS is not a good combination for stable and high-performance QLEDs. Recently, several attempts to replace ITO in optoelectronics were made. The candidates to replace ITO are Al-doped ZnO, Ti-doped In_2O_3 , and W-doped In_2O_3 (IWO) due to the desirable properties of high mobility, low sheet resistance, and high transmittance.^{15–17} Among the alternatives to ITO, IWO is considered as a suitable transparent electrode for the QLEDs. Tungsten (W) dopants in the In_2O_3 can generate an abundance of electron carriers due to the W^{6+} substitutions in the In^{3+} sites.¹⁸ As a result, the IWO requires less dopant than ITO, which can improve the impurity scattering effect. Therefore, IWO films can have a higher carrier concentration and higher mobility than ITO films. Moreover, the fabrication temperature for the highly transparent and conductive IWO film is lower than that of the ITO film.¹⁹

Meanwhile, there are many reports to suggest an alternative to PEDOT:PSS in QLEDs. Transition metal oxides (TMOs) are proposed as an HIL for the device because TMOs do not have acidic and hygroscopic properties. TMOs films may be formed using a solution coating process as well as the vacuum sputtering process. Vanadium oxide (V_2O_5), molybdenum oxide (MoO_3), nickel oxide (NiO), and copper oxide (CuO) have been used as a HIL in QLEDs.^{20–23} QLEDs with TMOs as the HIL

^aDepartment of Advanced Materials Engineering for Information and Electronics, Kyung Hee University, 1732 Deogyong-daero, Giheung-gu, Yongin, Gyeonggi-do 17104, Republic of Korea. E-mail: junkang@khu.ac.kr; Tel: +82-31-201-3324

^bInstitute of Physics and Applied Physics, Yonsei University, 50 Yonsei-ro, Seodaemun-gu, Seoul 03722, Republic of Korea

^cSchool of Advanced Materials & Engineering, Sungkyunkwan University, 2066 Seobu-ro, Jangan-gu, Suwon, Gyeonggi-do 16419, Republic of Korea



exhibited superior characteristics including stability upon exposure to oxygen, hydrogen, and heat.²⁴ Also, the adhesion force of V_2O_5 is strong enough to form a stable thin film on a substrate.²⁵ Therefore, the IWO transparent electrode and V_2O_5 HIL could be a suitable combination for developing the high-performance and inorganic QLEDs.

In this study, we fabricated inorganic QLEDs with the IWO transparent electrode and V_2O_5 HIL. The hole injection mechanism from the IWO electrode into the V_2O_5 HIL was investigated using ultraviolet photoelectron spectroscopy (UPS), and we found gap states inside the band gap of V_2O_5 . The gap states can provide a hole carrier injection pathway through the wide band gap of the V_2O_5 HIL. The hole injection characteristics between the IWO and V_2O_5 was investigated by characterizing a hole-only device (HOD), and efficient hole injection was observed. Conventional normal-structured QLEDs were fabricated successfully on a glass substrate with the IWO transparent electrode and V_2O_5 HIL. Our result suggests that the IWO transparent electrode and V_2O_5 HIL could be a good combination for the production of high-performance and inorganic QLEDs.

Experiments

We fabricated conventional-structured QLED devices on IWO electrodes with inorganic V_2O_5 HILs. A 100 nm thick layer of IWO films were deposited on a glass substrate using a plot-scale ion plating system with IWO tablets (99 at% In_2O_3 – 1 at% W) at room temperature.²⁶ During deposition of the IWO film, the working pressure, DC power and Ar/O_2 flow rate were constantly maintained at 3 mTorr, 3000 W and 300/90 sccm, respectively.¹⁸ The V_2O_5 solution was prepared using vanadium oxtriisopropoxide (Alfa Aesar, 96%) and isopropyl alcohol at a volume ratio of 1 : 70.²⁰ The V_2O_5 HIL was spin-coated on the IWO surface at 3000 rpm for 30 s, followed by annealing at 150 °C for 30 min. Then poly[(9,9-dioctylfluorenyl-2,7-diyl)-co-(4,4'-(4-sec-butylphenyl)diphenylamine)] (TFB) was coated onto the V_2O_5 surface as a hole transport layer (HTL). The emissive layer of CdSe/ZnS QDs (Nanosquare, NSQDs-HOS) and the electron transport layer of ZnO (Avantama, N-10) were spin-coated onto the HTL. Finally, a 130 nm thick layer of aluminum (Al) cathode was deposited onto the device using a thermal evaporator with a shadow mask. The same procedure was used to fabricate the HOD. Interfacial electronic structures of the IWO, V_2O_5 , and TFB were measured using UPS (SPECS, PHOIBOS 150) with UV (He I) light sources. High-resolution transmission electron microscopy (HRTEM, JEOL, JEM-2100F) was used to investigate the cross-sectional structure of the device. The current–voltage (I – V) characteristics of HODs and current–voltage–luminance (I – V – L) characteristics of QLEDs were measured using the conventional measurement system (McScience, M6100).

Results and discussion

Fig. 1(a) shows the UPS spectra of IWO, IWO/TFB, IWO/ V_2O_5 , and IWO/ V_2O_5 /TFB at the secondary cutoff (SEC) and highest

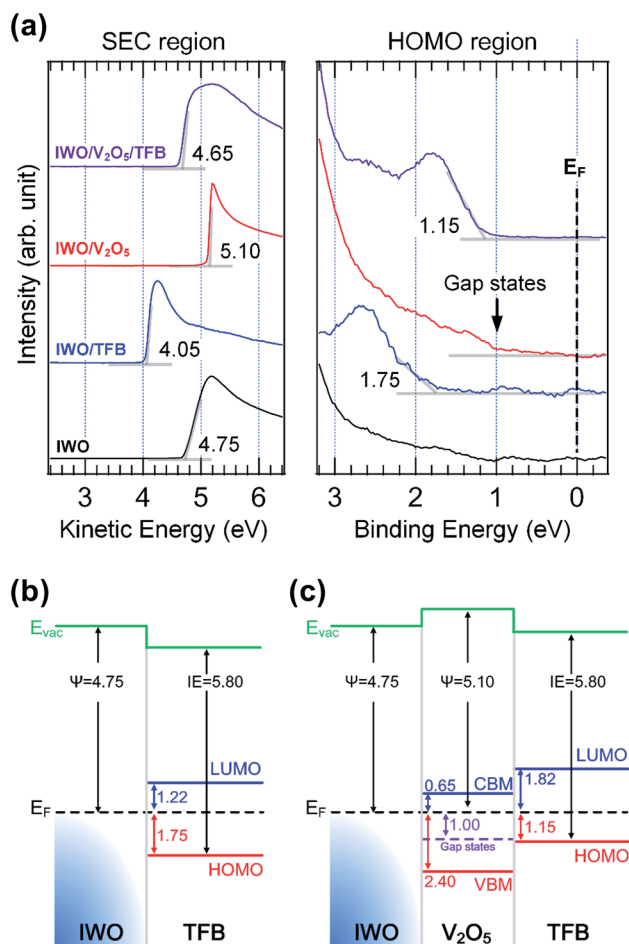
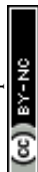


Fig. 1 (Color online) (a) measured UPS spectra of the IWO, IWO/TFB, IWO/ V_2O_5 , and IWO/ V_2O_5 /TFB at the SEC and HOMO region. Interfacial energy level diagram of (b) IWO/TFB and (c) IWO/ V_2O_5 /TFB.

occupied molecular orbital (HOMO) regions. All spectra were normalized and removed the Shirley-type background. The work function of the IWO was 4.75 eV as shown in the SEC region of the IWO spectrum. The HOMO level of TFB on IWO was measured to be 1.75 eV from the Fermi energy level (E_F) as shown in the HOMO region of the spectra. The valence band maximum (VBM) of V_2O_5 and the HOMO of TFB on V_2O_5 were 2.4 eV and 1.15 eV below the E_F . Notably, density of state (DOS) exists between the VBM and the E_F in the V_2O_5 spectrum. The DOS revealed the gap states of the V_2O_5 film, which play a key role to inject and transport hole carriers through the V_2O_5 film. The onset of the gap states was measured to be 1.0 eV below the E_F . The HOMO level of the TFB on V_2O_5 was measured as 1.15 eV from the E_F . According to the different under layers of TFB, the HOMO levels of TFB vary due to the specific interfacial electronic configurations. The interfacial energy level diagrams of the IWO/TFB and IWO/ V_2O_5 /TFB were evaluated from the UPS spectra, as shown in Fig. 1(b) and (c). The hole injection barrier from the IWO into the TFB is 1.75 eV, as shown in Fig. 1(b). The large hole injection barrier can be improved by inserting a thin V_2O_5 layer between the IWO and TFB. The VBM of V_2O_5 was located 2.4 eV below the E_F , while the gap states exist at the



1.0 eV below the E_F . Moreover, the HOMO level of the TFB on V_2O_5 was 1.15 eV below the E_F . The hole injection barrier from the IWO into the V_2O_5 is 1.0 eV by considering the gap states, and the hole injection barrier from V_2O_5 into TFB is 0.15 eV. Therefore, we can expect that the hole injection barrier can be reduced by inserting a thin layer of V_2O_5 between the IWO and TFB.

The HOD has been fabricated to evaluate the hole injection and transport process from the IWO into the TFB through the V_2O_5 inserting layer. As shown in the inset of Fig. 2, the structure of the HOD is composed of IWO/ V_2O_5 /TFB/Al layers. In this configuration, holes can easily flow from the IWO to Al electrodes, while electrons have difficulty flowing from Al to the IWO electrodes due to the high electron injection barrier. Therefore, the HOD is useful to evaluate the hole injection and transport behavior. Fig. 2 shows the current density–voltage (J – V) characteristics of the HOD. The slope of the J – V curve was calculated as ~ 1.5 at the low voltage region, which indicates that the ohmic conduction ($J \propto V$) is dominant. The slope changed to ~ 2.2 when the voltage exceeded 3 V, which indicates that the space charge limited conduction (SCLC, $J \propto V^2$) is dominant. Consistent with the interfacial energy level diagram of Fig. 1(c), holes can efficiently inject from the IWO into TFB through V_2O_5 . Moreover, the measured hole mobility was $27.8 \text{ cm}^2 \text{ V}^{-1} \text{ s}^{-1}$, which is high enough for the HIL layer. Therefore, the gap states of V_2O_5 play a key role in injecting hole carriers into the device.

Fig. 3(a) shows the schematic of the QLEDs with the IWO transparent electrode and V_2O_5 HIL. The IWO layer was sputtered on a glass substrate, and V_2O_5 , TFB, QDs, and ZnO layers were spin-coated on the IWO surface. Then Al was deposited using a thermal evaporator with a shadow mask. Fig. 3(b) shows the energy level diagram of the QLEDs. All energy levels were aligned according to the E_F . Holes can inject from the IWO into QDs through the gap states of V_2O_5 , and HOMO of the TFB. Although there is a possibility of charge generation effect by moving electrons from the HOMO of the TFB into the conduction band minimum (CBM) of V_2O_5 , it hardly occurs due to the high barrier from the HOMO of TFB to the CBM of V_2O_5 (1.8 eV).²⁷ Fig. 3(c) shows the cross-sectional HRTEM images of the QLEDs. Clearly, all IWO, V_2O_5 , TFB, QDs, ZnO, and Al layers were uniformly coated and well defined, as shown in the image.

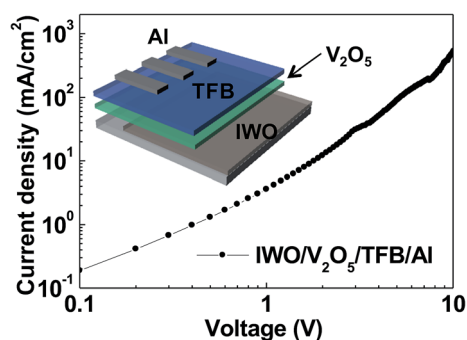


Fig. 2 (Color online) voltage–current density characteristic of the IWO/ V_2O_5 /TFB/Al HOD. The inset shows the schematic of the HOD.

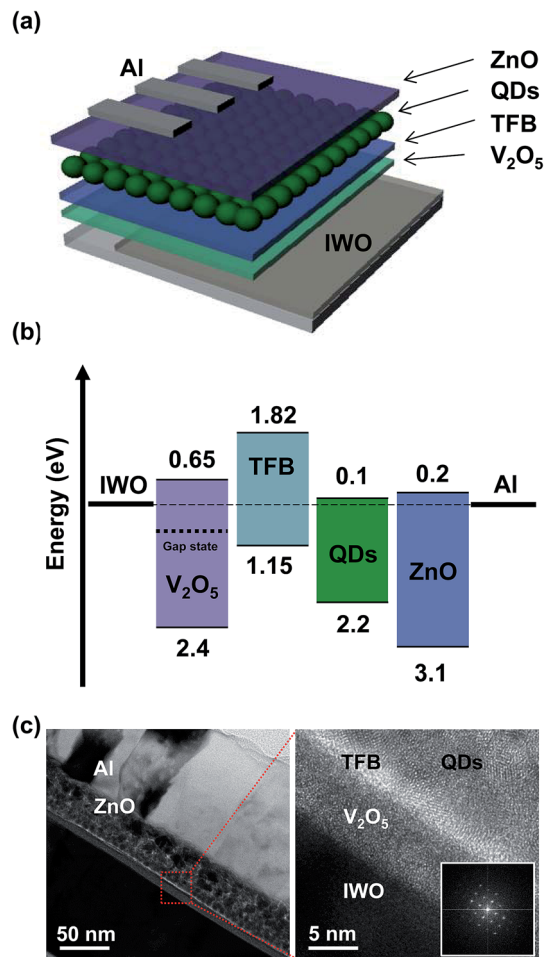


Fig. 3 (Color online) (a) schematic of the QLEDs on the IWO transparent electrode. (b) Energy level diagram, aligned to the E_F , of the QLEDs. The hole can be injected through the gap state of the V_2O_5 HIL. (c) Cross-sectional HRTEM images of the QLEDs. The inset shows the FFT pattern of the IWO.

The inset shows the Fast Fourier Transform (FFT) of the IWO film, which clearly indicated the crystalline structure of the IWO film with the (222) preferred orientation even though it was prepared at room temperature. Fig. 4(a) shows the normalized electroluminescence (EL) spectrum of the QLEDs with the IWO anode and V_2O_5 HIL. The emission peak of the spectrum was located at 536 nm, and the full-width at half maximum was measured as 30.5 nm. The inset shows a photographic image of the turned-on QLEDs. Fig. 4(b) shows the luminance and current density as a function of applied voltage. The maximum luminance was measured as 9443.5 cd m^{-2} at the applied voltage of 7.6 V. The turned-on voltage was 2.6 V. The maximum luminance of QLEDs with ITO/PEDOT:PSS/TFB structure showed the maximum luminance of 9710.6 cd m^{-2} and turn-on voltage of 3.5 V. The current density of QLEDs expressed the behavior of hole and electron current through the device. Fig. 4(c) shows the current density vs. voltage in a log scale of each axis. Under the voltage of 2.2 V, the slope of J – V was ~ 1.5 , which indicates that the ohmic conduction was dominant. The slope was changed to ~ 4.2 at the applied voltages between 2.2



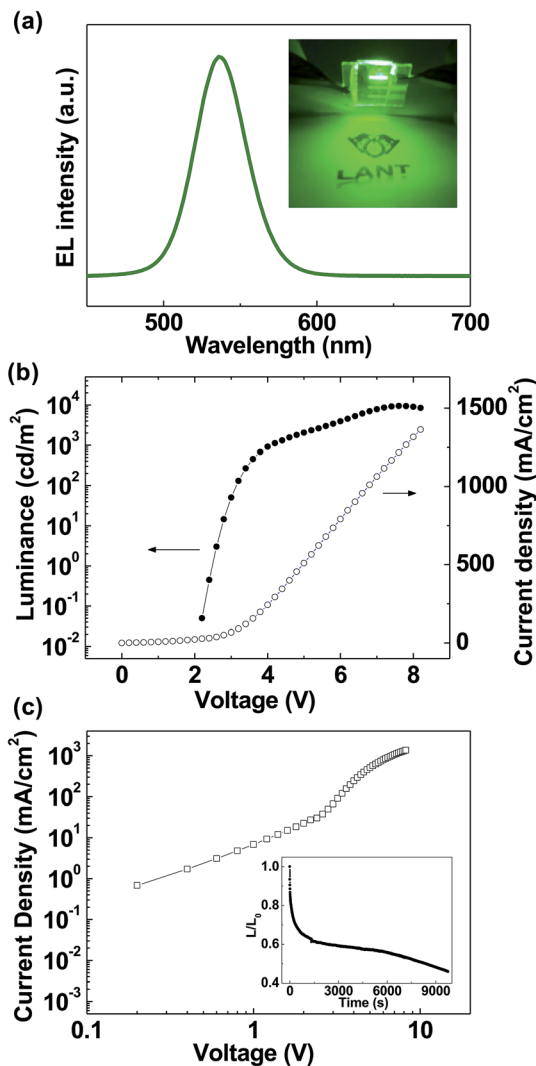


Fig. 4 (Color online) (a) EL characteristics of QLEDs on a glass/IWO substrate. The inset shows the turned-on QLEDs. (b) Luminance and current density vs. applied voltage curves. (c) J - V curve in a log-scale. The inset shows the life-time characteristics of the QLEDs.

and 4.6 V. In this range, the trap limited SCLC ($J \propto V^n$, $n > 2$) was dominant. Above the voltage of 4.6 V, the slope approached ~ 2.1 , which shows the SCLC ($J \propto V^2$) behavior is dominant. The inset shows the life-time characteristics of the QLEDs with IWO/ V_2O_5 . The initial luminance was 1000 cd m^{-2} , and the curves were measured under ambient conditions at room temperature. Consistent with the interfacial energy level diagram shown in Fig. 1(c), the QLEDs with the IWO anode and V_2O_5 HIL worked well due to the hole injection through the gap states of V_2O_5 .

Conclusion

In conclusion, the hole injection mechanism from the IWO electrode into the TFB through the V_2O_5 HIL was investigated in detail using UPS. Complete interfacial energy level diagrams of the IWO/TFB and IWO/ V_2O_5 /TFB were evaluated from the UPS spectra. We found gap states inside the band gap of V_2O_5 ,

located at 1.0 eV below the E_F . These gap states can provide a hole injection pathway, and the hole injection behavior was confirmed by characterizing the HOD. Conventional-structured QLEDs were successfully fabricated on a glass substrate with the IWO transparent electrode and V_2O_5 HIL. The maximum luminance of the device was measured as 9443.5 cd m^{-2} . Our result suggests that the IWO electrode and V_2O_5 HIL are a good combination for developing high-performance and inorganic QLEDs.

Conflicts of interest

There are no conflicts to declare.

Acknowledgements

This work was supported by a research project grant from the National Research Foundation of Korea (NRF-2016R1D1A1B03932144).

References

- 1 J. R. Manders, L. Qian, A. Titov, J. Hyvonen, J. T. Scott, K. P. Acharya, Y. Yang, W. Cao, Y. Zheng, J. Xue and P. H. Holloway, *J. Soc. Inf. Disp.*, 2015, **23**, 523.
- 2 B. S. Mashford, M. Stevenson, Z. Popovic, C. Hamilton, Z. Zhou, C. Breen, J. Steckel, V. Bulovic, M. Bawendi, S. C. Sullivan and P. T. Kazlas, *Nat. Photonics*, 2013, **7**, 407.
- 3 H. Shen, Q. Lin, W. Cao, C. Yang, N. T. Shewmon, H. Wang, J. Niu, L. S. Li and J. Xue, *Nanoscale*, 2017, **9**, 13583.
- 4 X. Yang, E. Mutlugun, C. Dang, K. Dev, Y. Gao, S. T. Tan, X. W. Sun and H. V. Demir, *ACS Nano*, 2014, **8**, 8224.
- 5 S. Baskoutas and A. F. Terzis, *J. Appl. Phys.*, 2006, **99**, 013708.
- 6 K. H. Lee, C. Y. Han, H. D. Kang, H. Ko, C. Lee, J. Lee, N. Myoung, S. Y. Yim and H. Yang, *ACS Nano*, 2015, **9**, 10941.
- 7 J. Kwak, W. K. Bae, D. Lee, I. Park, J. Lim, M. Park, H. Cho, H. Woo, D. Y. Yoon, K. Char, S. Lee and C. Lee, *Nano Lett.*, 2012, **12**, 2362.
- 8 W. K. Bae, J. Lim, D. Lee, M. Park, H. Lee, J. Kwak, K. Char, C. Lee and S. Lee, *Adv. Mater.*, 2014, **26**, 6387.
- 9 J. Meyer, T. Winkler, S. Hamwi, S. Schmale, H. H. Johannes, T. Weimann, P. Hinze, W. Kowlasky and T. Riedl, *Adv. Mater.*, 2008, **20**, 3839.
- 10 K. Schulze, B. Maennig, K. Leo, Y. Tomita, C. May, J. Hupkes, E. Brier, D. Reinold and P. Bauerle, *Appl. Phys. Lett.*, 2007, **91**, 073521.
- 11 K. Utsumi, O. Matsunaga and T. Takahata, *Thin Solid Films*, 1998, **334**, 30.
- 12 W. Deng, T. Ohgi, H. Nejo and D. Fujita, *Appl. Phys. A*, 2001, **72**, 595.
- 13 X. Dai, Z. Zhang, Y. Jin, Y. Niu, H. Cao, X. Liang, L. Chen, J. Wang and X. Peng, *Nature*, 2014, **515**, 96.
- 14 X. Yang, E. Mutlugun, Y. Zhao, Y. Gao, K. S. Leck, Y. Ma, L. Ke, S. T. Tan, H. V. Demir and X. W. Sun, *Small*, 2013, **10**, 247.
- 15 X. Jiang, F. L. Wong, M. K. Fung and S. T. Lee, *Appl. Phys. Lett.*, 2003, **83**, 1875.



- 16 J. A. Jeong, Y. J. Jeon, S. S. Kim, B. K. Kim, K. B. Chung and H. K. Kim, *Sol. Energy Mater. Sol. Cells*, 2014, **122**, 241.
- 17 Z. Lu, F. Meng, Y. Cui, J. Shi, Z. Feng and Z. Liu, *J. Phys. D: Appl. Phys.*, 2013, **46**, 075103.
- 18 J. Kim, J. Lee, S. M. Jo, B. D. Chin, J. Baek, K. Ahn, S. J. Kang and H. Kim, *Sci. Rep.*, 2018, **8**, 12019.
- 19 F. Meng, J. Shi, Z. Liu, Y. Cui, Z. Lu and Z. Feng, *Sol. Energy Mater. Sol. Cells*, 2014, **122**, 70.
- 20 S. M. Lee, D. Shin, N. K. Cho, Y. Yi and S. J. Kang, *Curr. Appl. Phys.*, 2017, **17**, 442.
- 21 C. Zheng, F. Li, Q. Zeng, H. Hu and T. Guo, *Thin Solid Films*, 2019, **669**, 387.
- 22 Y. Zhang, S. Wang, L. Chen, Y. Fang, H. Shen and Z. Du, *Org. Electron.*, 2017, **44**, 189.
- 23 T. Ding, X. Yang, L. Bai, Y. Zhao, K. E. Fong, N. Wang, H. V. Demir and X. W. Sun, *Org. Electron.*, 2015, **26**, 245.
- 24 H. T. Nguyen, N. D. Nguyen and S. Lee, *Nanotechnology*, 2013, **24**, 115201.
- 25 B. A. Bhat, G. R. Khan and K. Asokan, *RSC Adv.*, 2015, **5**, 52602.
- 26 J.-H. Kim, H.-J. Seok, H.-J. Seo, T.-Y. Seong, J. H. Heo, S.-H. Lim, K.-J. Ahn and H.-K. Kim, *Nanoscale*, 2018, **10**, 20587.
- 27 J. Meyer, K. Zilberberg, T. Riedl and A. Kahn, *J. Appl. Phys.*, 2011, **110**, 033710.

